

Mirror Symmetry Breaking and Network Formation in Achiral Polycatenars with Thioether Tail

Mohamed Alaasar,^{*[a, b]} Ahmed F. Darweesh,^[b] Xiaoqian Cai,^[c] Feng Liu,^[c] and Carsten Tschierske^{*[a]}

Abstract: Mirror symmetry breaking in systems composed of achiral molecules is of importance for the design of functional materials for technological applications as well as for the understanding of the mechanisms of spontaneous emergence of chirality. Herein, we report the design and molecular self-assembly of two series of rod-like achiral polycatenar molecules derived from a π -conjugated 5,5'-diphenyl-2,2'-bithiophene core with a fork-like triple alkoxyated end and a variable single alkylthio chain at the other end. In both series of liquid crystalline materials, differing in the chain length at the trialkoxyated end, helical self-assembly of the π -con-

jugated rods in networks occurs, leading to wide temperature ranges (> 200 K) of bicontinuous cubic network phases, in some cases being stable even around ambient temperatures. The achiral bicontinuous cubic $la\bar{3}d$ phase (gyroid) is replaced upon alkylthio chain elongation by a spontaneous mirror symmetry broken bicontinuous cubic phase ($I23$) and a chiral isotropic liquid phase (Iso_1^{*k}). Further chain elongation results in removing the $I23$ phase and the re-appearance of the $la\bar{3}d$ phase with different pitch lengths. In the second series an additional tetragonal phase separates the two cubic phase types.

Introduction

Since their discovery in 1888, liquid crystalline (LC) materials have undergone an astonishing development to the present day. They are of great interest as stimuli-responsive and switchable optical materials in displays,^[1] photonics,^[2] in sensor,^[3,4] and telecommunication applications,^[5] for ion conducting materials,^[6] in organic electronics and photovoltaics,^[7–9] and in biomedicine for targeted drug delivery.^[10–12] LC are usually composed of an anisometric rigid rod-like or disc-like core, providing orientational order, combined with a distinct number of flexible alkyl chains, providing the mobility. In most cases the alkyl chains are connected by ether linkages to the rigid units. In contrast to these alkyl(oxy) chains the related

alkylthio chains were much less used, but nevertheless replacing alkyl or alkoxy by alkylthio chains can often lead to interesting new properties. For example, hexa(alkylthio) triphenylenes were the first columnar LC for which photoconducting properties were reported.^[13] Alkylthio tails were also used to induce columnar and cubic phase formation in bent-core mesogens.^[14] 4-(Alkylthio)benzoic acids lead to enhanced cybotactic nematic phase ranges compared to the related 4-*n*-alkoxy-substituted compounds in hydrogen-bonded supramolecular systems.^[15,16] More recently, the thioether linkage was shown to be advantageous for the design of mesogenic dimers with wide ranges of the twist-bend nematic phase.^[17,18] Herein the effect of replacing alkyloxy chains of polycatenar LCs by alkylsulfanyl (alkylthio) chains on LC self-assembly and spontaneous mirror symmetry breaking is reported. Polycatenar LCs are rod-like mesogens with multi terminal chains, providing a transition between lamellar and columnar self-assembly by modification of the chain volume. These polycatenars have received significant interests due to their rich mesomorphism including nematic, smectic, bicontinuous cubic (Cub_{bi}) and columnar mesophases.^[19–27] Cub_{bi} phases are optically isotropic LC with cubic 3D lattice, in most cases occurring at the transition between lamellar and columnar modes of self-assembly as a result of the increasing interface curvature upon growing alkyl chain volume.^[28–33] The double gyroid with space group $la\bar{3}d$ is the most common type of Cub_{bi} phases composed of two interwoven, but not interconnected networks with three way junctions (Figure 1a,c).^[34–37] In the case of polycatenars the networks are formed by the π -conjugated rods, whereas the flexible chains fill the space between the networks. Because the rods are organized almost perpendicular to the local network direction, their π -systems can overlap and these networks provide 3D conduction pathways for charge

[a] Dr. M. Alaasar, Prof. C. Tschierske
Institute of Chemistry
Martin Luther University Halle-Wittenberg
Kurt Mothes Str. 2, 06120 Halle (Saale) (Germany)
E-mail: mohamed.alaasar@chemie.uni-halle.de
carsten.tschierske@chemie.uni-halle.de

[b] Dr. M. Alaasar, Prof. A. F. Darweesh
Department of Chemistry
Faculty of Science
Cairo University, Giza (Egypt)

[c] X. Cai, Prof. F. Liu
State Key Laboratory for Mechanical Behavior of Materials
Shaanxi International Research Center for Soft Matter
Xi'an Jiaotong University, Xi'an 710049 (P. R. China)

Supporting information for this article is available on the WWW under <https://doi.org/10.1002/chem.202102226>

© 2021 The Authors. Chemistry - A European Journal published by Wiley-VCH GmbH. This is an open access article under the terms of the Creative Commons Attribution Non-Commercial NoDerivs License, which permits use and distribution in any medium, provided the original work is properly cited, the use is non-commercial and no modifications or adaptations are made.

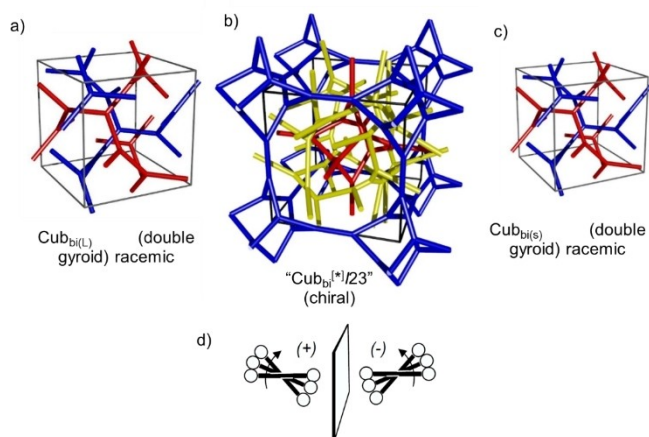


Figure 1. a, c) The double network gyroid with $Ia\bar{3}d$ space group and b) the more complex triple network of the mirror symmetry broken $I23$ phase, the two networks (blue and red) in a,c) are enantiomorphous, in b) are identical and different from the yellow one; d) the development of the helical twist by the clashing of end groups attached to rod-like cores in the networks; the twist between the molecules along the network increases from a) to c), resulting in a transition from the long pitch $Ia\bar{3}d_{(L)}$ (Low twist) via the $I23$ lattice to the short pitch $Ia\bar{3}d_{(S)}$ (high twist) phase. a–c) Reprinted with permission from Ref. [42, 52].

transportation (see Figure 1), which makes these Cub_{bi} phases interesting for organic electronics applications.^[7,38]

In this organization of the π -conjugated rods perpendicular to the networks the rod-like units cannot align perfectly parallel, because the overcrowding of the ends by the multiple alkyl chains induces a twist (Figure 1d). Due to the network structure the twist sense is synchronized along the networks,^[59] leading to a helical network with uniform chirality along the individual nets. In the gyroid type Cub_{bi} phase with $Ia\bar{3}d$ space group the twist is opposite in the two interwoven networks and thus cancels out to an overall achiral structure.^[39,40] However, recently it was found that there is another type of Cub_{bi} phase which is chiral and forms conglomerates of chiral domains with opposite handedness.^[39–51] This is due to the triple network structure of this Cub_{bi} phase with space group $I23$ (Figure 1b),^[52] previously known as $Im\bar{3}m$.^[53–57] In this case the network chirality cannot cancel out and a conglomerate of chiral domains is observed. It is noted that the transition from the achiral to the ambidextrous chiral cubic phase might not only be due to the transition from a racemic double network to a scalemic triple network phase. It is also possible that this transition is accompanied by a transition from an enantiophilic (racemate forming) self-assembly in the double gyroid composed of two intrinsically chiral enantiomorphous networks, to an enantiophobic (conglomerate forming) mode of self-assembly in the $I23$ phase with three achiral networks. In the latter case the enantiophobic helix-helix interaction becomes dominating, thus leading to identical chirality in all three networks. Importantly, spontaneous mirror symmetry breaking and optical activity can be even retained in the ambidextrous chiral isotropic liquid phases ($Iso_1^{[k]}$) occurring adjacent to the Cub_{bi} phases with helical network structure.^[58–61]

The directed design of materials with application relevant nano-scale morphologies and molecular properties for applications requires the fundamental understanding of the structure property relationships. Especially the design of cubic phases and helical network structures showing spontaneous mirror symmetry breaking is still at the infancy and requires systematic studies.^[62] In order to investigate the effect of alkythio chains on the helical self-assembly of polycatenar compounds new non-symmetric tetracatenar mesogens based on the π -conjugated rod-like 5,5'-diphenyl 2,2'-dithiophene unit (**A10/n** and **A6/n**) were designed, synthesized, investigated and compared with related alkoxy substituted compounds (Scheme 1).

Experimental

Synthesis

The synthesis of the tetracatenar phenol **6** (Scheme 1) was conducted in a similar manner to that reported before by Suzuki type boronate cross-coupling reaction,^[58] while the synthesis of the 4-alkylthiobenzoic acids **8** was performed by Williamson etherification of 4-mercaptobenzoic acid with different alkylbromides followed by hydrolysis.^[15] In the final step acylation of **6** with the benzoyl chlorides **8** using triethylamine and a catalytic amount of pyridine led to the target compounds **A10/n** and **A6/n**, as described in the Supporting Information.

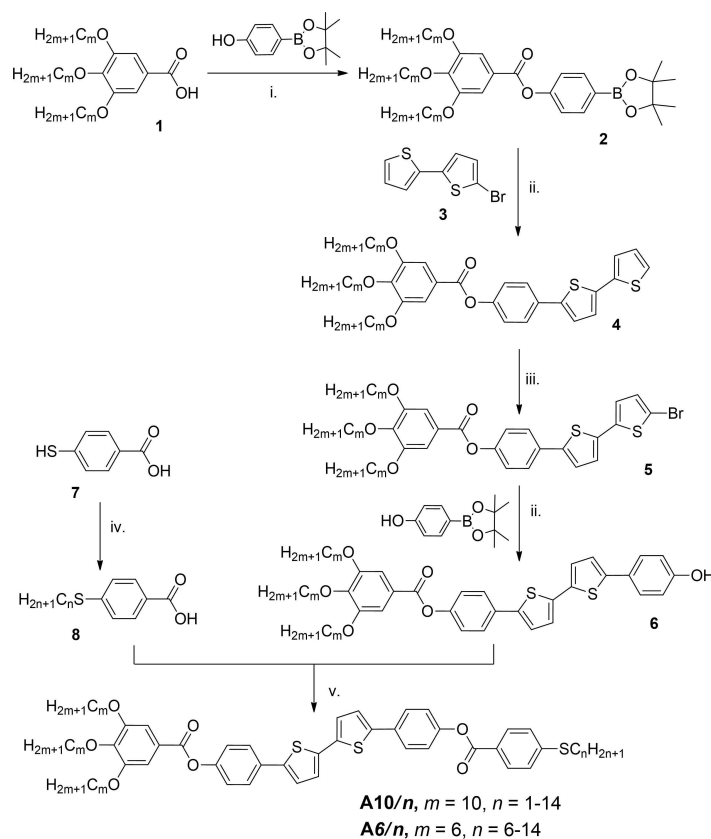
Investigation methods

Investigation of the obtained materials was conducted by polarizing optical microscopy (POM) (Optiphot 2, Nikon microscope with a Mettler FP82HT heating stage), differential scanning calorimetry (DSC-7 and DSC-8000 Perkin Elmer, 10 K min⁻¹ peak temperatures quoted in Table 1), and X-ray diffraction (XRD). In-house XRD was carried out using $Cu_{K\alpha}$ radiation and a Vantec 500 area detector. High-resolution small/wide-angle X-ray scattering (SAXS/WAXS) experiments were recorded on Beamline BL16B1 at Shanghai Synchrotron Radiation Facility, SSRF. Experiments were carried out on samples in 1 mm glass capillaries under the control of a modified Linkam hot stage with a thermal stability within 0.2 °C. The Pilatus 2M detector was applied in the experiments. θ calibration and linearization were testified by using several orders of layer reflections from silver behenate and a series of n -alkanes.

Results and Discussion

Cubic phases

As can be concluded from Figure 2 and Table 1 all the synthesized compounds exhibit wide LCs phase ranges with the type of mesophases and their ranges depending on the length of the chains at both ends of the molecules. All of the polycatenars in series **A10/n** with three terminal decyloxy chains at one end of the rod-like molecule and a growing alkythio chain at the other end exhibit Cub_{bi} phases as indicated from POM and XRD measurements. The cubic phases are characterized by their uniformly dark appearance between crossed polarizers as they are optically isotropic. The transition



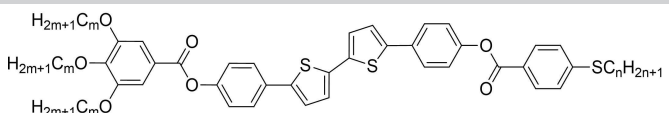
Scheme 1. Synthesis of polycatenars under investigation. Reagents and conditions: i) DCC, DMAP, DCM, RT, stirring; ii) $[\text{Pd}(\text{PPh}_3)_4]$, THF/sat. NaHCO_3 -solution, reflux; iii) NBS, THF, RT, absence of light; iv) 1) absolute EtOH, KOH, $\text{H}_{2n+1}\text{C}_n\text{Br}$, 2) NaOH solution, reflux, 3) H^+ ; v) 1) SOCl_2 , 2) Triethylamine, pyridine, DCM, reflux.

from the isotropic liquid to the cubic phase on cooling is identified by a sudden increase of viscosity which is associated with a DSC peak (Table 1 and Figure 3).

For all homologues, there is a 6–12 K supercooling of the Iso–Cub transition compared to the Cub–Iso transition temperature on heating which is a typical feature of cubic LC phases with 3D periodicity (Table 1).^[63] A series of sharp SAXS peaks appear at the Iso–Cub_{bi} transition, replacing the single diffuse scattering observed in the isotropic liquid state. Based on the positions of the scattering maxima two types of Cub_{bi} phases can be distinguished. For the short and long chain compounds the two most intense scatters in the SAXS patterns can be indexed to the (211) and (220) reflections of an $la\bar{3}d$ lattice with lattice parameters a_{Cub} around 11 nm (Figure 4a). This assignment to an $la\bar{3}d$ lattice is in line with the absence of chiral domains in this achiral Cub_{bi} phase (see Figure 5g,h, top right/bottom left). In contrast, all compounds with an intermediate chain length form conglomerate of chiral domains (Figure 5d–f). For this Cub_{bi} phase the SAXS pattern can be indexed to the (321), (400), (330), (411) and (420) scatterings of an $I23$ lattice, as shown in Figure 4d for compound **A6/10** as an example. The lattice parameter a_{Cub} is between 17.0 and 17.3 nm for compounds **A10/n**, whereas for the compounds **A6/n** with shorter apex chains it is 15.5–16.0 nm. At the $la\bar{3}d$ to $I23$ transitions there is a 46–58% increase of the lattice parameter,

in line with the proposed transition from a double to a triple network structure. The electron density (ED) map of this Cub_{bi}^[36]/ $I23$ phase, reconstructed based on the diffraction intensities show the complex triple network structure of the $I23$ phase of **A6/10** as example (Figure 4d).

While in the series **A10/n** the Cub_{bi}–Iso transition temperature decreases with growing length of the alkylthio chain, the phase range of the Cub_{bi} phase at first decreases by chain elongation ($n = 1 \rightarrow 8$) then it remains constant for $n = 10$ and 12 and starts to increase again for $n = 14$ (Figure 2). Interestingly, the $la\bar{3}d$ phase exhibited by the shorter homologues (**A10/1** and **A10/2**) is completely removed and replaced by the $I23$ phase upon chain elongation (for $n = 4 \rightarrow 10$) and then it re-emerges again for derivatives with $n \geq 12$. Therefore, it appears that there are two types of the $la\bar{3}d$ phase, one is a long pitch (low twist) $la\bar{3}d_{(L)}$, favoured by short chains and the other one is a short pitch (high twist) $la\bar{3}d_{(S)}$, favoured by long chains and the two types are separated by the $I23$ phase for medium chains. This sequence $la\bar{3}d_{(L)}$ – $I23$ – $la\bar{3}d_{(S)}$ is typically observed for homologous series of compounds forming Cub_{bi} phases, as for example in the ANBC-*ns* and BABH-*ns*,^[34,64–68] and recently also found for tapered 5,5'-diphenyl-2,2'-dithiophenes upon increasing the volume of the apex substituent or increasing the size of an alicyclic ring at the apex.^[41,44]

Table 1. Phase transitions of compounds **A10/n** and **A6/n**.^[a]


Comp.	<i>m</i>	<i>n</i>	Phase transitions <i>T</i> /°C [ΔH /kJ mol ⁻¹]	<i>a</i> _{cub} /nm (<i>T</i> /°C)	Φ /°	3 <i>m</i> + <i>n</i>
A10/1	10	1	H: Cr < 20 Cub _{bi} / <i>la</i> $\bar{3}d$ 212 [1.3] Iso C: Iso 202 [1.0] Cub _{bi} / <i>la</i> $\bar{3}d$ Cr < 20	11.5 (150)	7.8	31
A10/2	10	2	H: Cr < 20 Cub _{bi} / <i>la</i> $\bar{3}d$ 205 [1.1] Iso C: Iso 200 [< 0.1] Iso ^[sk] 195 [0.8] Cub _{bi} / <i>la</i> $\bar{3}d$	11.6 (150)	7.7	32
A10/4	10	4	H: Cr1 94 [14.3] Cr2 104 [3.1] Cub _{bi} / <i>I23</i> 190 [1.3] Iso C: Iso 189 [0.1] Iso ^[sk] 184 [0.7] Cub _{bi} / <i>I23</i>	17.0 (150)	8.2	34
A10/6	10	6	H: Cr 116 [40.6] Cub _{bi} / <i>I23</i> 190 [2.5] Iso C: Iso 182 [< 0.1] Iso ^[sk] 181 [1.9] Cub _{bi} / <i>I23</i> 57 [22.2] Cr	17.3 (170)	8.1	36
A10/8	10	8	H: Cr 115 [37.9] Cub _{bi} / <i>I23</i> 182 [2.3] Iso C: Iso 176 [< 0.1] Iso ^[sk] 174 [1.9] Cub _{bi} / <i>I23</i> 72 [23.80] Cr	–	–	38
A10/10	10	10	H: Cr 126 [43.7] Cub _{bi} / <i>I23</i> 181 [2.6] Iso C: Iso 172 [1.9] Cub _{bi} / <i>I23</i> 96 [39.6] Cr	17.2 (150)	8.2	40
A10/12	10	12	H: Cr 126 [44.6] Cub _{bi} / <i>la</i> $\bar{3}d$ 181 [2.7] Iso C: Iso 172 [1.9] Cub _{bi} / <i>la</i> $\bar{3}d$ 96 [41.1] Cr	10.9 (150)	8.2	42
A10/14	10	14	H: Cr 89 [37.0] Cub _{bi} / <i>la</i> $\bar{3}d$ 172 [2.8] Iso C: Iso 162 [1.9] Cub _{bi} / <i>la</i> $\bar{3}d$ 70 [39.3] Cr	10.9 (150)	8.2	44
A6/6	6	6	H: Cr 129 [34.2] Cub _{bi} / <i>la</i> $\bar{3}d$ 207 [2.2] Iso C: Iso 204 [0.3] Iso ^[sk] 190 [0.8] Cub _{bi} / <i>la</i> $\bar{3}d$ 78 [28.3] Cr	10.6 (150)	8.5	24
A6/8	6	8	H: Cr 121 [35.2] Cub _{bi} / <i>la</i> $\bar{3}d$ 198 [2.1] Iso C: Iso 193 [0.4] Iso ^[sk] 178 [0.5] Cub _{bi} / <i>la</i> $\bar{3}d$ 80 [23.2] Cr	10.6 (150)	8.5	26
A6/10	6	10	H: Cr 133 [50.7] Tet 155 [-] Cub _{bi} / <i>I23</i> 192 [2.4] Iso C: Iso 190 [0.4] Iso ^[sk] 181 [0.8] Tet 85 [39.1] Cr	15.5 (150)	9.0	28
A6/12	6	12	H: Cr 85 [46.8] Cub _{bi} / <i>I23</i> 193 [4.5] Iso C: Iso 185 [< 0.1] Iso ^[sk] 183 [1.6] Cub _{bi} / <i>I23</i> 82 [36.2] Cr	15.8 (140)	8.8	30
A6/14	6	14	H: Cr 103 [36.6] Cub _{bi} / <i>I23</i> 191 [3.4] Iso C: Iso 181 [2.4] Cub _{bi} / <i>I23</i> 87 [40.5] Cr	16.0 (140)	8.7	32

[a] Peak temperatures as determined from 2nd heating (upper lines) and 2nd cooling (lower lines) DSC scans with rate 10 K/min.; Abbreviations: Cr = crystalline solid; Iso = isotropic liquid; Iso^[sk] spontaneous symmetry broken ambidextrous chiral isotropic liquid phase; Cub_{bi}/*la* $\bar{3}d$ = achiral bicontinuous cubic phase with *la* $\bar{3}d$ space group; Cub_{bi}/*I23* = ambidextrous chiral bicontinuous cubic phase with *I23* space group; Tet = non-cubic 3D phase with tetragonal symmetry; *a*_{cub} = lattice parameter of the cubic phase; Φ = twist angle between adjacent rafts of molecules in the networks of the *la* $\bar{3}d$ -phases; $\Phi(la\bar{3}d) = 70.5^\circ / [0.354a_{cub} / 0.45 \text{ nm}]$, $\Phi(I23) = 90^\circ / [0.290a_{cub} / 0.45 \text{ nm}]$,^[52] see Table S7 for the full set of structural data and Tables S1–S6 and Figures S3, S4 for XRD data.

As shown in Table 1 all observed Cub_{bi} phases represent thermodynamically stable (enantiotropic) phases. For the shortest two homologues **A10/1** and **A10/2** the *la* $\bar{3}d$ phase is observed both on heating and cooling over very wide temperature range (> 200 K) without any crystallization even after storing the sample for several months. This makes these materials of potential interest for applications which require stable cubic phases around ambient temperature.

While there is a large jump of *a*_{cub} at the *la* $\bar{3}d$ -*I23* transitions, the cubic lattice parameter remains almost constant in the *la* $\bar{3}d$ ranges of the short and long chain compounds. Within the *I23* range *a*_{cub} first increases and then slightly decreases and between the two *la* $\bar{3}d$ ranges in the series of compounds **A10/n** there is a difference of 0.6–0.7 nm with larger values for the compounds with shorter chains (Figure 6a). This inverse dependence of the lattice parameter on the chain length can be interpreted as an effect of the chain volume on the twist between the molecules. Accordingly, for molecules with shorter chains the twist should be smaller, and with growing chain length it should increase. As the distance between the junctions is defined by *a*_{cub} as well as the valency of junctions and the twist between them, there are geometric restrictions for the

twist between the molecules along the networks as the molecular rods have to arrive almost parallel to each other at each junction. This is in line with the development of the twist angles in the distinct Cub_{bi} phases (see Table 1 and Figure 6a) calculated from the lattice parameters and the molecular dimensions according to the equations developed in Ref. [52] (see Table S7). In the series **A10/n** the twist angle (Φ) increases from 7.8° in the *la* $\bar{3}d$ phase of the shortest homologue **A10/1**, approaches a value of 8.2° in the *I23* phase, and this twist is retained in the *la* $\bar{3}d$ phases of the longest homologues. The development of a chiral *I23* phase in the contact region between the achiral *la* $\bar{3}d$ phases of the short compound **A10/2** and the longest compound **A10/14** (Figure 5g–i) confirms that the *la* $\bar{3}d$ phases of the two compounds are different from each other, i.e. they represent long pitch *la* $\bar{3}d_{(L)}$ and short pitch *la* $\bar{3}d_{(S)}$ phases, respectively.^[41,44,46]

The effect of temperature on the development of the helical twist was also investigated in the cubic phase ranges of those compounds located around at the Cub_{bi}/*la* $\bar{3}d$ -*I23* transitions. As shown in Figure 6b, the helical twist significantly increases from *n* = 2 to *n* = 4 at the transition *la* $\bar{3}d_{(L)}$ -*I23*, while the *T*-dependence is only small. In contrast, for the compounds with long

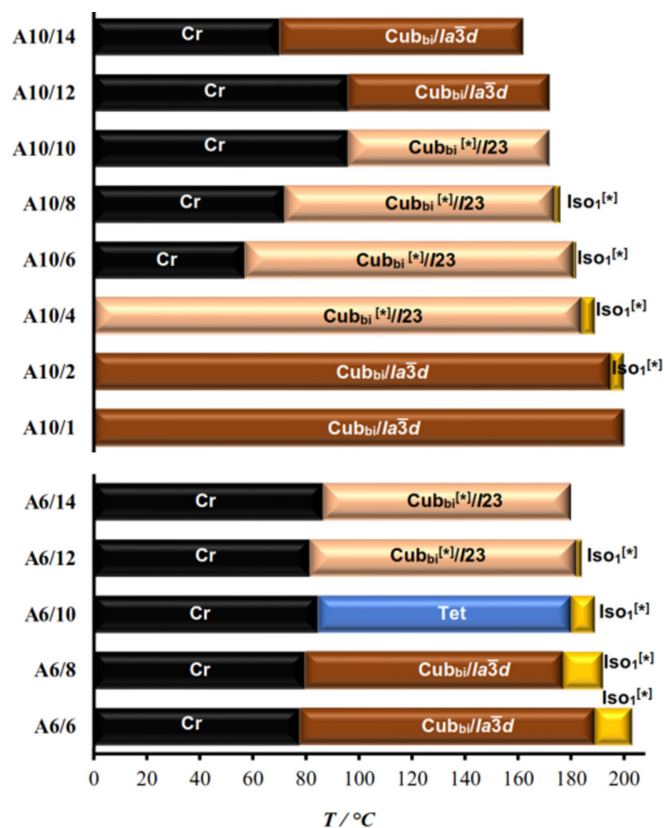


Figure 2. Phase transitions of the polycatenar compounds **A10/n** and **A6/n** as observed on cooling with a rate of 10 K min^{-1} .

chains ($n=10,12$), located around the $I23 \rightarrow Ia\bar{3}d_{(s)}$ transition, there is a significant temperature dependence of the twist, growing with rising temperature, as expected for thermal chain expansion. However, there is only a surprisingly small difference between the curves recorded for the $Ia\bar{3}d_{(s)}$ and $I23$ phases of these two homologues (magenta and dark blue in Fig.6b). The strong temperature dependence of Φ in these two cases (especially if further extrapolated to lower T) could be explained by a change of the chain flexibility. At low temperature there is less conformational disorder and the elongation of the n -alkylthio chain mainly contributes to the elongation of the molecule, thus reducing the twist between the molecules. With growing chain disorder at higher temperature, the contribution to the molecular length decreases, whereas the contribution to the lateral expansion of the n -alkyl chain grows and Φ increases. For shorter RS chains ($n=2,4$) this temperature effect on chain conformation is smaller (red and light blue in Fig.6b).

Decreasing the length of the chains at the trisubstituted end from $m=10$ (**A10/n**) to $m=6$ results in the analogue series **A6/n** (Table 1, Figure 2). This structural modification changes slightly the transition temperatures and retains the Cub_{bi} phases observed in the series **A10/n**. However, in this series the chiral $Iso_1^{[*]}$ phase is observed for compounds with $n=6-12$ in relatively wide temperature ranges compared to the **A10/n** series, meaning that the formation of the $Iso_1^{[*]}$ phase is supported by short chains. As expected, in the series **A6/n** the

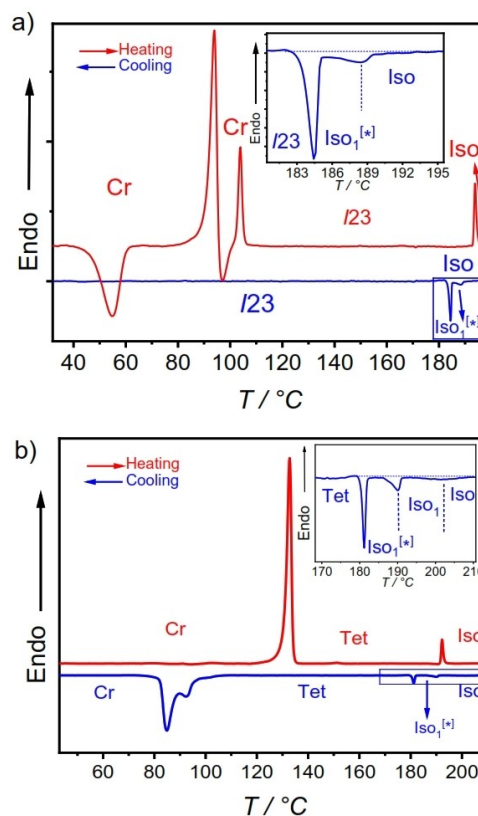


Figure 3. DSC heating and cooling traces recorded at 10 K min^{-1} of compounds: a) **A10/4** and b) **A6/10**. The insets in a) and b) show enlarged scale for the $Iso-Iso_1^{[*]}-LC$ transition on cooling.

transition from $Ia\bar{3}d$ to the triple network $Cub_{bi}^{[*]}/I23$ phase requires longer apex chains. The short pitch $Ia\bar{3}d_{(s)}$ region is not reached (Figure 2) in this series because the apex chain length is limited to $n=14$.

Interesting is the effect of the total chain volume on the Cub_{bi} phase type. Whereas in the series **A10/n** a total chain volume corresponding to 32–34 CH_2 units is required for the $Ia\bar{3}d \rightarrow I23$ transition, this transition requires only 26–28 CH_2 units, i.e. 8 CH_2 units less in the series **A6/n** (Table 1). This means that, though chain elongation of all three chains at the dendritic end provides a much larger increase of chain volume than elongation of the single apex chain by the same number of C-atoms, there is a stronger effect of the chain volume added to the apex compared to the effect of the same chain volume change at the branched end. A possible explanation could be that the RS chains at the apex allow a larger conformational flexibility, thus effectively requiring more space than the conformationally more restricted RO chains at the tapered end. Indeed for related tetracatenar compound with an RO instead of the RS apex chains (**B10/n**) the $Ia\bar{3}d \rightarrow I23$ transition takes place at 34 CH_2 units and for **B6/n** at 30–32 units.^[69,70] These values are much closer to each other due to the comparable chain flexibility of the RO chains at both ends.

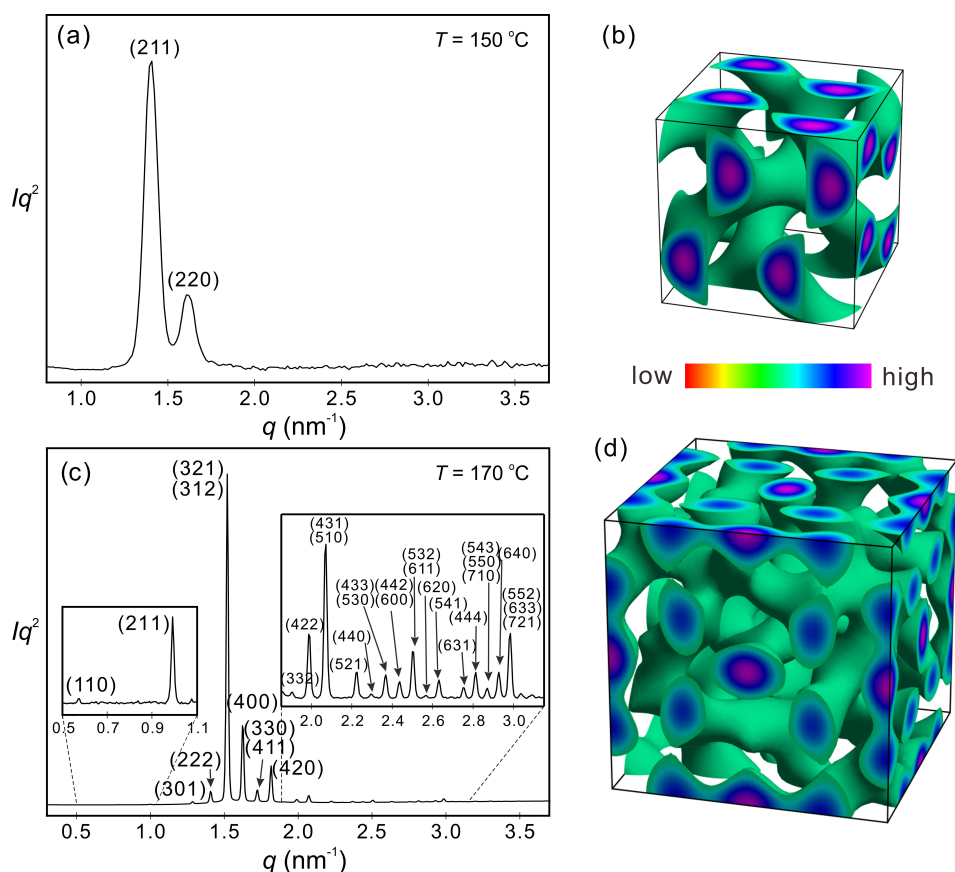


Figure 4. SAXS diffractogram as recorded on heating: a) at 150 °C in the $\text{Cub}_{\text{bi}}/Ia\bar{3}d$ phase of **A10/14**; b) Reconstructed electron density map of **A10/14** in $\text{Cub}_{\text{bi}}/Ia\bar{3}d$ phase. c) at 170 °C in the $\text{Cub}_{\text{bi}}^{[*]}/I23$ phase of **A6/10** (for numerical data, see Table S2); d) Reconstructed electron density map of **A6/10** in $\text{Cub}_{\text{bi}}^{[*]}/I23$ phase; for details of the ED reconstruction, see Section 4 and Figure S5 in the Supporting Information.

Non-cubic 3D phases

Another difference between series **A10/n** and **A6/n** is that in the latter case an additional birefringent mesophase occurs at the $Ia\bar{3}d$ - $I23$ transition upon chain elongation, which is missing in the series **A10/n**. On heating **A6/10** under crossed polarizers a transition from the crystalline phase to a highly viscous isotropic mesophase takes place at $T \sim 133$ °C. Under slightly uncrossed polarizers a conglomerate of dark and bright domains can be easily detected which invert their brightness by inversion of the direction of the polarizers, indicating the chirality of this phase i.e. it is a chiral $\text{Cub}_{\text{bi}}^{[*]}/I23$ phase. The chirality of $\text{Cub}_{\text{bi}}^{[*]}/I23$ is lost on further heating at the transition to the fluid isotropic liquid (Iso). On cooling **A6/10** from the achiral Iso phase with a rate of 10 K min^{-1} the chirality emerges at ~ 181 °C, while the phase remains highly fluid as in ordinary liquids, indicating the formation of an $\text{Iso}_1^{[*]}$ phase which exists over ~ 7 K and transforms on further cooling to a birefringent 3D phase (Figure 7). Such birefringent mesophases with non-cubic 3D-lattice were often observed in the vicinity of Cub_{bi} phases formed by polycatenar molecules and could have tetragonal, orthorhombic or rhombohedral lattices,^[42,64,71–74] the most prominent being the SmQ phase,^[53,75] and the S4 phase. The 3D phase of **A6/10** could be indexed to a tetragonal lattice

(Tet, see Figure S4). The lattice parameters of the tetragonal phase are $a = 14.5$ nm and $c = 18.9$ nm which are close to $a_{\text{cub}} = 15.5$ nm in the $I23$ phase. This suggests that the tetragonal phase is likely to result from a stretching of the $I23$ lattice along one direction. The very similar unit cell volumes (3.72 nm³ for $I23$ and 3.95 nm³ for Tet, see Table S7) and the optical investigations, showing that the birefringence is relatively small, are in line with this explanation. In the temperature range of all Cub_{bi} phases as well as in the Tet phase of **A6/10**, the WAXS is completely diffuse with a maximum around 0.45 nm which confirms LCs phases without fixed positions of the individual molecules (see Figure S3).

Upon fast cooling (≥ 20 K min^{-1}) the Tet phase remains over a temperature range of ~ 96 K until the onset of crystallization at ~ 85 °C (Figure 7c). With cooling rates below 10 K min^{-1} the Cub_{bi} phase develops together with the Tet phase (Figure 7b) and slowly replaces the Tet phase. This means that the Tet phase is metastable with respect to the non-distorted $\text{Cub}_{\text{bi}}^{[*]}/I23$ phase. If the Tet phase is chiral or achiral cannot be decided, because the linear birefringence of the Tet phase is much larger than the possible effects of optical rotation. However, it is likely to be a chiral phase as it occurs between two mirror symmetry broken phases, $\text{Iso}_1^{[*]}$ and $\text{Cub}_{\text{bi}}^{[*]}/I23$.

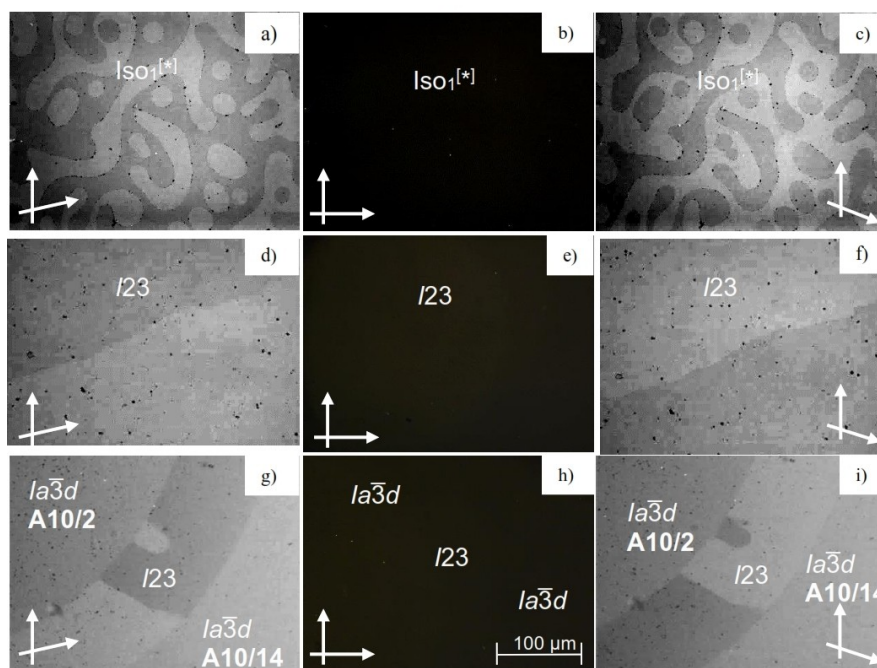


Figure 5. Chiral domains observed in: a,c) $Iso_1^{[*]}$ phase of **A10/2** at 198 °C; d,f) $I23$ phase of **A10/4** at 150 °C; g,i) the induced $I23$ phase in the contact regions between the achiral $Ia\bar{3}d$ phases of **A10/2** and **A10/14** at 170 °C. The textures in left and right columns are between slightly rotated polarizers and in the middle column (b,e,h) are under fully (90°) crossed polarizers and therefore appear completely dark.

Mirror symmetry broken isotropic liquids

Another interesting feature of series **A10/n** is the observation of an additional transition between two different types of liquid phases on cooling of **A10/2**–**A10/8** before the transition to the cubic phases (Table 1, Figure 3). On cooling compound **A10/4**, as example, a broad feature occurs in the DSC traces in the temperature range of the isotropic liquid phase, indicating a liquid-liquid transition (Figure 3a). This broad transition is followed by a sharp peak indicating the transition to the cubic phase, associated with a sudden increase of the viscosity. In the temperature range of the broad liquid-liquid transition the emergence of mirror symmetry breaking could be detected by the appearance of chiral domains under slightly uncrossed polarizers (Figure 5a–c). Therefore, this mirror symmetry broken isotropic liquid phase is assigned as $Iso_1^{[*]}$ phase and considered as a kind of percolated liquid with a dynamic helical network structure.^[45] Interestingly, the $Iso_1^{[*]}$ phase appears beside the achiral gyroid $Ia\bar{3}d$ phase for **A10/2** as well as beside the ambidextrous chiral $I23$ phase for **A10/4**–**A10/8**. Its range decreases with chain elongation ($n=2\rightarrow 8$) and is completely removed for compounds **A10/n** with $n\geq 10$. This $Iso_1^{[*]}$ phase is also formed by compounds **A6/6**–**A6/12**, again associated with the $Ia\bar{3}d$ to $I23$ transition. As in the series **A10/n** the $Iso_1^{[*]}$ phase is metastable, but the monotropic phase region observed on cooling before the transition to the Cub_{bi} (and Tet) phase is broader (up to 14 K). The development of this phase from the achiral isotropic liquid (Iso) apparently takes place in two steps in this case, at about 202 °C there is the maximum of a very broad and weak DSC feature, which we attribute to the Iso- Iso_1

transition, associated with the growth of helical aggregates fusing to local networks (Figure 3b). This Iso-Iso $_1$ transition is most clearly seen for **A6/10**, being directly at the $Ia\bar{3}d$ to $I23$ transition and it is not so clear for the other compounds **A6/n**. The peak at 190 °C is associated with the onset of long-range chirality synchronization in the Iso $_1$ range (Iso $_1$ -Iso $_1^{[*]}$ transition) and the much larger peak at 180 °C indicates the transition to the long range periodic Tet phase. That the mirror symmetry broken $Iso_1^{[*]}$ phase appears in some cases above the achiral double gyroid $Ia\bar{3}d$ phase can be understood by thermal chain expansion at the transition to the isotropic state. As this is known to induce the transition from $Ia\bar{3}d_{(L)}$ to $I23$ (see above) it is postulated that the local structure in the $Iso_1^{[*]}$ phase is $I23$ -like, leading to chiral conglomerate formation.

Comparison with related alkoxy substituted polycatenars

In Figure 8 some of the compounds synthesized herein are compared with their analogues having alkoxy instead of the alkylthio chains (**Bm/n**).^[39,58] As shown in Figure 8 the same phase types and phase sequences are observed in both series. However, replacing S by O increases the $Iso_1^{[*]}$ ranges on the expense of the Cub_{bi} phases. For the pair **A10/1**, **B10/1** an increased stability of the cubic phase by replacing O by S is observed, whereas for the compounds with longer chains at the apex ($n=6, 10$) this order is reversed. The main effects of replacing ether by thioether linkages are a decreased C–S–C bonding angle (99°) compared to C–O–C (114°),^[76] a changed molecular shape from almost rod-like to more bent and an

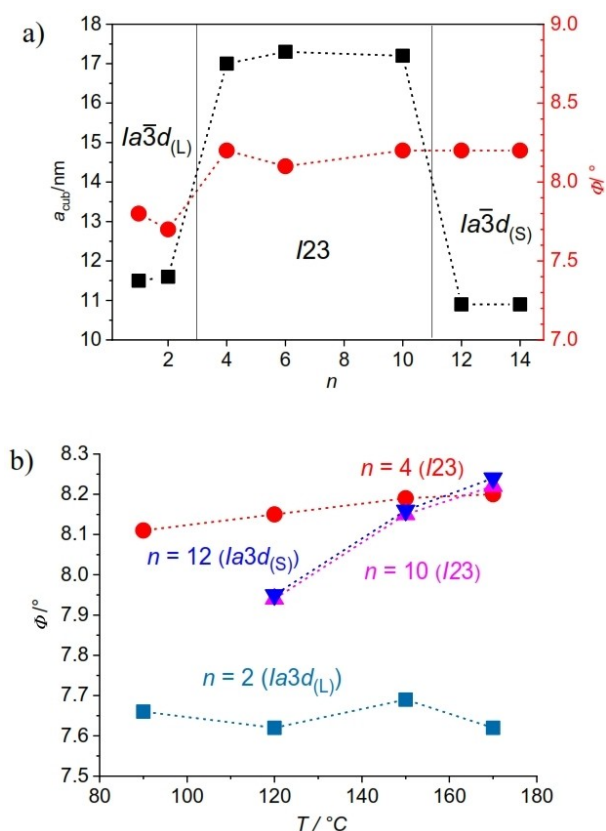


Figure 6. Investigation of the cubic phases of compounds **A10/n**. a) Dependence of the twist angle (ϕ) and lattice parameter (a_{cub}) on RS chain length (n); the twist angle (ϕ) was calculated according to: $\phi(la\bar{3}d) = 70.5^\circ / [0.354a_{\text{cub}}/0.45 \text{ nm}]$ and $\phi(I23) = 90^\circ / [0.290a_{\text{cub}}/0.45 \text{ nm}]$;^[52] b) dependence of ϕ on the temperature.

increased C–S bond length (1.82 nm) compared to C–O (1.45 nm).^[76] The latter decreases the rotational barrier around the C–S bonds compared to the C–O bonds (O–CH₃: 11.3 kJ mol⁻¹; S–CH₃: 8.4 kJ mol⁻¹) and thus increases conformational chain mobility.^[77,78] Increased conformational chain disorder of arylthioethers is also supported by the decreased conjugation of S with the benzene ring if compared with related arylethers.^[79] Moreover, the reduced electronegativity of

S compared to O leads to reduced dipolar intermolecular interactions whereas its larger electric polarizability provides stronger dispersion forces between the thioethers. In cases where the conformation is biased, as in heterocycles, a strong mesophase stabilizing effect of S compared to O of about 20 K per S was observed.^[80] In contrast, the enhanced conformational flexibility around the C–S bonds reduces the stability of LC phases if an alkyl chain is attached to a core unit via a thioether linkage.^[81,82] The increased stability of the LC phases of the short chain compounds **Am/n** can be attributed to the increased attractive dispersion forces provided by the larger sulphur. For longer chains this stabilizing effect of S is compensated by its mesophase destabilizing effect due to the increased conformational chain mobility and therefore the effect of replacing O by S is reversed for the longer homologues. The increased chain mobility is likely to also contribute to the reduced melting points and reduced crystallization tendency of the thioethers, which besides the suppression of birefringent phases causes a widening of the Cub_{bi} ranges in all cases.^[15] (see Table 2).

Summary and Conclusions

The design, synthesis, and investigation of two new series of 5,5'-diphenyl-2,2'-bithiophene based polycatenars terminated with thioether chains at the monosubstituted apex is reported. The effect of the RS chain length on the development of helical and mirror symmetry broken soft matter network phases was investigated and compared to the related analogues terminated with alkoxy chains. Depending on the length of the terminal chain, the synthesized materials exhibit different types of LC phase. Very wide ranges of cubic phases, even around room temperature makes these compounds good candidates for technological applications. Spontaneous mirror symmetry breaking based on chirality synchronization in helical networks was observed in the triple network cubic phase with $I23$ symmetry and in the isotropic liquid phase (Iso₁^[*]).^[59] The mirror symmetry broken isotropic liquid is observed in both series of compounds (**A10/n** and **A6/n**) for medium and short chain compounds. For the series **A10/n** a phase sequence $la\bar{3}char/Ox00AFnotimplementedd_{(L)}-I23-la\bar{3}d_{(S)}$ with a chiral $I23$ phase between two achiral $la\bar{3}d$ phases is observed with chain

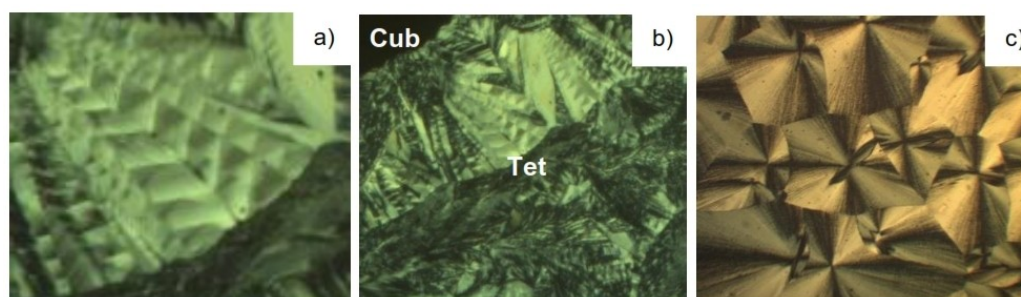


Figure 7. Optical textures obtained for compound **A6/10**: a) and b) with a cooling rate of 10 K/min; a) Tet phase at 174 °C; b) Tet + Cub at 125 °C and c) Tet phase at 125 °C using a cooling rate of 20 K/min. Due to the very different appearance it is not clear from these investigations if the 3D phase formed on rapid cooling is the same as on fast cooling only with a different alignment or a slightly different 3D phase.

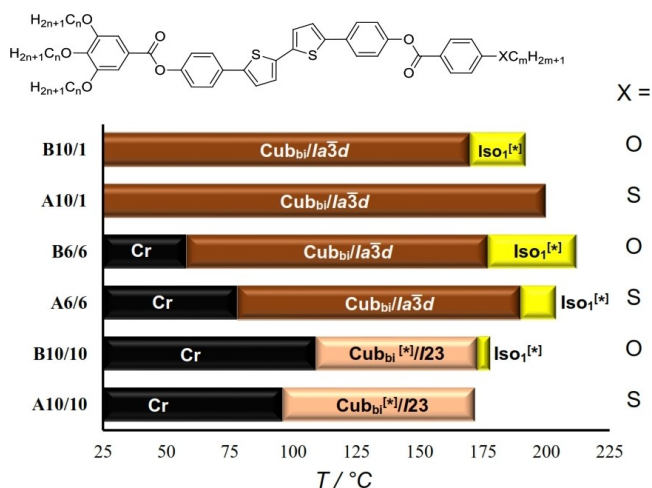


Figure 8. Phase transitions of the polycatenar compounds **A10/1**, **A10/10**, **A6/6** and their related analogues **B10/1**,^[39] **B10/10**,^[39] and **B6/6**^[58] as observed on cooling (DSC with rate 10 K min⁻¹), for abbreviations see Table 1.

elongation. Mirror symmetry breaking was also induced upon mixing two components forming achiral $Ia\bar{3}d$ phases.^[50] At the $Ia\bar{3}d_{(L)}$ -I23 transition upon chain elongation a tetragonal phase (Tet) is observed in the series **A6/n**, which is suggested to represent a deformed version of the I23 lattice. The precise structure of this Tet phase and related birefringent 3D phases found in other series of polycatenar compounds require further studies.

Acknowledgements

M. Alaasar acknowledges the German Research Foundation (DFG) for the financial support (AL2378/1-1, 424355983). A. F. Darweesh acknowledges the support by the Alexander von Humboldt Foundation for the research fellowship at Martin Luther University Halle-Wittenberg, Germany. F. Liu thanks the financial support from the National Natural Science Foundation of China (21761132033, 21374086). The authors are grateful to Beamline BL16B1 at SSRF (Shanghai Synchrotron Radiation Facility, China) for providing the beamtime. Open Access funding enabled and organized by Projekt DEAL.

Conflict of Interest

The authors declare no conflict of interest.

Keywords: bithophene · chirality · cubic phases · liquid crystals · mirror symmetry breaking · soft matter

- [1] J. A. Castellano, The Story of Liquid Crystal Displays and the Creation of an Industry, World Scientific, Singapore 2005.
[2] L. Wang, Q. Li, *Adv. Funct. Mater.* **2016**, *26*, 10–28.

- [3] W. Goodby, P. J. Collings, T. Kato, C. Tschierske, H. Gleeson, P. Raynes, Handbook of Liquid Crystals, 2nd ed., Wiley-VCH, Weinheim, Germany 2014.
[4] Q. Li, Nanoscience with Liquid Crystals. – From Self-Organized Nanostructures to Applications, Springer, Cham, Switzerland 2014.
[5] R. Jakoby, A. Gaebler, C. Weickmann, *Crystals* **2020**, *10*, 514–560.
[6] H. Iino, J. Hanna, *Polym. J.* **2017**, *49*, 23–30.
[7] T. Kato, J. Uchida, T. Ichikawa, T. Sakamoto, *Angew. Chem. Int. Ed.* **2018**, *57*, 4355–4371; *Angew. Chem.* **2018**, *130*, 4438–4455.
[8] M. O'Neill, S. M. Kelly, *Adv. Mater.* **2011**, *23*, 566–584.
[9] S. Sergeev, W. Pisula, Y. H. Geerts, *Chem. Soc. Rev.* **2007**, *36*, 1902–1929.
[10] E. Bukusoglu, M. B. Pantoja, P. C. Mushenheim, X. Wang, N. L. Abbott, *Annu. Rev. Chem. Biomol. Eng.* **2016**, *7*, 163–196.
[11] T. Yasuda, H. Ooi, J. Morita, Y. Akama, K. Minoura, M. Funahashi, T. Shimomura, T. Kato, *Adv. Funct. Mater.* **2009**, *19*, 411–419.
[12] Y. Chen, P. Ma, S. Gui, *BioMed Res. Int.* **2014**, *2014*, 1–12.
[13] D. Adam, P. Schuhmachert, J. Sllmerer, L. Hiussllngt, K. Siemensmeyert, K. H. Etbacht, H. Ringsdorf, D. Haarer, *Nature* **1994**, *371*, 141–143.
[14] S. Kang, M. Harada, X. Li, M. Tokita, J. Watanabe, *Soft Matter* **2012**, *8*, 1916–1922.
[15] Y. Arakawa, Y. Sasaki, K. Igawa, H. Tsuji, *New J. Chem.* **2017**, *41*, 6514–6522.
[16] Y. Arakawa, Y. Sasaki, H. Tsuji, *Chem. Lett.* **2017**, *46*, 1657–1659.
[17] Y. Arakawa, Y. Ishida, H. Tsuji, *Chem. Eur. J.* **2020**, *26*, 3767–3775.
[18] Y. Arakawa, K. Komatsu, Y. Ishida, H. Tsuji, *Liq. Cryst.* **2021**, *48*, 641–652.
[19] W. Weissflog, in Handbook of Liquid Crystals, 2nd ed. (Eds: J. W. Goodby, J. P. Collings, T. Kato, C. Tschierske, H. F. Gleeson, P. Raynes), Wiley-VCH, Weinheim, Germany 2014, pp. 89–174.
[20] D. W. Bruce, *Acc. Chem. Res.* **2000**, *33*, 831–840.
[21] H. T. Nguyen, C. Destrade, J. Malthete, *Adv. Mater.* **1997**, *9*, 375–388.
[22] N. T. Nguyen, C. Destrade, J. Malthete, *Liq. Cryst.* **1990**, *8*, 797–811.
[23] I. Nishiyama, *Chem. Rec.* **2009**, *9*, 340–355.
[24] M. Yoneya, *Chem. Rec.* **2011**, *11*, 66–76.
[25] A. Yoshizawa, *Polym. J.* **2012**, *44*, 490–502.
[26] M. Alaasar, S. Poppe, *Liq. Cryst.* **2019**, *47*, 939–949.
[27] M. Alaasar, *J. Mol. Liq.* **2021**, *341*, 117341–117347.
[28] S. Hyde, S. Andersson, K. Larsson, Z. Blum, T. Landh, S. Lidin, B. W. Ninham, The language of shape. The role of curvature in condensed matter: Physics, Chemistry and Biology, Elsevier, Amsterdam 1997.
[29] A. J. Meuler, M. A. Hillmyer, F. S. Bates, **2009**, *42*, 7221–7250.
[30] J. M. Seddon, R. H. Templer, Polymorphism in Lipid-Water Systems. In Handbook of Biological Physics; Lipowsky, R. and E. Sackmann, Eds.; Elsevier: Amsterdam, 1995; Vol. 1, pp 97–160.
[31] G. Ungar, F. Liu, X. B. Zeng, in Handbook of Liquid Crystals (Eds: W. Goodby, P. J. Collings, T. Kato, C. Tschierske, H. Gleeson, P. Raynes), Wiley-VCH, Weinheim, Germany 2014.
[32] C. Tschierske, *J. Mater. Chem.* **1998**, *8*, 1485–1508.
[33] L. Hag, S. L. Gras, C. E. Conn, C. J. Drummond, *Chem. Soc. Rev.* **2017**, *46*, 2705–2731.
[34] A. H. Schoen, *Interface Focus* **2012**, *2*, 658–668.
[35] S. Kutsumizu, *Isr. J. Chem.* **2012**, *52*, 844–853.
[36] L. Han, S. Che, *Adv. Mater.* **2018**, *30*, 1705708–1705729.
[37] M. L. Lynch, P. T. Spicer, Bicontinuous Liquid Crystals, CRC Press, Taylor & Francis Group, Boca Raton, FL 2005.
[38] O. Kwon, X. Cai, W. Qu, F. Liu, J. Szydlowska, E. Gorecka, M. J. Han, D. K. Yoon, S. Poppe, C. Tschierske, *Adv. Funct. Mater.* **2021**, *31*, 2102271–212280.
[39] C. Dressel, F. Liu, M. Prehm, X. B. Zeng, G. Ungar, C. Tschierske, *Angew. Chem. Int. Ed.* **2014**, *53*, 13115–13120; *Angew. Chem.* **2014**, *126*, 13331–13336.
[40] Y. Cao, M. Alaasar, A. Nallapaneni, M. Salamończyk, P. Marinko, E. Gorecka, C. Tschierske, F. Liu, N. Vaupotič, C. Zhu, *Phys. Rev. Lett.* **2020**, *125*, 027801–027806.
[41] C. Dressel, T. Reppe, S. Poppe, M. Prehm, H. Lu, X. Zeng, G. Ungar, C. Tschierske, *Adv. Funct. Mater.* **2020**, *30*, 2004353–2004368.
[42] M. Alaasar, J.-C. Schmidt, X. Cai, F. Liu, C. Tschierske, *J. Mol. Liq.* **2021**, *332*, 115870–115884.
[43] M. Alaasar, S. Poppe, Q. Dong, F. Liu, C. Tschierske, *Chem. Commun.* **2016**, *52*, 13869–13872.
[44] T. Reppe, C. Dressel, S. Poppe, C. Tschierske, *Chem. Commun.* **2020**, *56*, 711–714.
[45] T. Reppe, S. Poppe, X. Cai, Y. Cao, F. Liu, C. Tschierske, *Chem. Sci.* **2020**, *11*, 5902–5908.
[46] T. Reppe, S. Poppe, C. Tschierske, *Chem. Eur. J.* **2020**, *26*, 16066–16079.

- [47] M. Alaasar, S. Poppe, Q. Dong, F. Liu, C. Tschierske, *Angew. Chem. Int. Ed.* **2017**, *56*, 10801–10805; *Angew. Chem.* **2017**, *129*, 10941–10945.
- [48] M. Alaasar, S. Poppe, Y. Cao, C. Chen, F. Liu, C. Zhu, C. Tschierske, *J. Mater. Chem. C* **2020**, *8*, 12902–12916.
- [49] T. Reppe, C. Dressel, S. Poppe, A. Eremin, C. Tschierske, *Adv. Opt. Mater.* **2020**, 2001572–2001589.
- [50] S. Kutsumizu, S. Miisako, Y. Miwa, M. Kitagawa, Y. Yamamura, K. Saito, *Phys. Chem. Chem. Phys.* **2016**, *18*, 17341–17344.
- [51] J. M. Wolska, J. Wilk, D. Pocięcha, J. Mieczkowski, E. Gorecka, *Chem. Eur. J.* **2017**, *23*, 6853–6857.
- [52] X. Zeng, G. Ungar, *J. Mater. Chem. C* **2020**, *8*, 5389–5398.
- [53] A.-M. Levelut, M. Clerc, *Liq. Cryst.* **1998**, *24*, 105–115.
- [54] X. Zeng, G. Ungar, M. Imperor-Clerc, *Nat. Mater.* **2005**, *4*, 562–567.
- [55] Alternative models of this Cub_b phase being composed of only one network and spherical aggregates have also been proposed, see ref. 63, 64.
- [56] K. Saito, Y. Yamamura, Y. Miwa, S. Kutsumizu, *Phys. Chem. Chem. Phys.* **2016**, *18*, 3280–3284.
- [57] N. Vaupotic, M. Salamonczyk, J. Matraszek, M. Vogrin, D. Pocięcha, E. Gorecka, *Phys. Chem. Chem. Phys.* **2020**, *22*, 12814–12820.
- [58] C. Dressel, T. Reppe, M. Prehm, M. Brautzsch, C. Tschierske, *Nat. Chem.* **2014**, *6*, 971–977.
- [59] C. Tschierske, G. Ungar, *ChemPhysChem* **2016**, *17*, 1224–1251.
- [60] C. Tschierske, C. Dressel, *Symmetry* **2020**, *12*, 1098–1128.
- [61] M. Alaasar, M. Prehm, Y. Cao, F. Liu, C. Tschierske, *Angew. Chem. Int. Ed.* **2016**, *128*, 320–324.
- [62] C. Tschierske, *Liq. Cryst.* **2018**, *45*, 2221–2252.
- [63] A. Kummar, V. Molinero, *J. Phys. Chem. B* **2018**, *122*, 4758–4770.
- [64] a) G. W. Gray, B. Jones, F. Marson, *J. Chem. Soc.* **1957**, 393–401; b) H. Schubert, J. Hauschild, D. Demus, S. Hoffmann, *Z. Chem.* **1978**, *18*, 256.
- [65] Y. Yamamura, Y. Nakazawa, S. Kutsumizu, K. Saito, *Phys. Chem. Chem. Phys.* **2019**, *21*, 23705–23712.
- [66] S. Kutsumizu, K. Morita, T. Ichikawa, S. Yano, S. Nojima, T. Yamaguchi, *Liq. Cryst.* **2002**, *29*, 1447–1458.
- [67] D. Demus, D. Marzotko, N. K. Sharma, A. Wiegeleben, *Kryst. Tech.* **1980**, *15*, 331–339.
- [68] S. Kutsumizu, K. Morita, T. Ichikawa, S. Yano, S. Nojima, T. Yamaguchi, *Liq. Cryst.* **2002**, *29*, 1447–1458.
- [69] C. Dressel, PhD Thesis, University Halle, **2015**.
- [70] T. Reppe, Master Thesis, University Hlle, **2015**.
- [71] G. E. Schröder-Turk, A. Fogden, S. T. Hyde, *Eur. Phys. J. B* **2006**, *54*, 509–524.
- [72] A. Fogden, S. T. Hyde, *Eur. Phys. J. B* **1999**, *7*, 91–104.
- [73] C. A. Tyler, D. C. Morse, *Phys. Rev. Lett.* **2005**, *94*, 208302–208305.
- [74] J. Matraszek, D. Pocięcha, N. Vaupotic, M. Salamonczyk, M. Vogrine, E. Gorecka, *Soft Matter* **2020**, *16*, 3882–3885.
- [75] H. Lu, X. Zeng, G. Ungar, C. Dressel, C. Tschierske, *Angew. Chem. Int. Ed.* **2018**, *57*, 2835–2840; *Angew. Chem.* **2018**, *130*, 2885–2890.
- [76] T. Sakaizumi, M. Namikawa, O. Ohashi, *J. Mol. Struct.* **1995**, *345*, 189–195.
- [77] J. Hine, *Reaktivität und Mechanismus in der Organischen Chemie*, Thieme Stuttgart, **1960**.
- [78] F. G. Riddell, *The conformational analysis of Heterocyclic compounds*, Academic Press, **1980**.
- [79] V. F. Petrov, V. A. Vinkurov, V. V. Belyav, *Mol. Cryst. Liq. Cryst.* **2010**, *518*, 40–59.
- [80] C. Tschierske, D. Joachimi, H.-M. Vorbrod, H. Zschke, A. Wiegeleben, A. Hauser, D. Demus, *Liq. Cryst.* **1989**, *5*, 177–190.
- [81] E. Kleinpeter, H. Köhler, A. Lunow, C. Tschierske, H. Zschke, *Tetrahedron* **1988**, *44*, 1609–1612.
- [82] Y. Arakawa, S. Kang, H. Tsuji, J. Watanabe, G.-I. Konishi, *RSC Adv.* **2016**, *6*, 16568–16574.

Manuscript received: June 21, 2021

Accepted manuscript online: September 20, 2021

Version of record online: October 7, 2021